



## Regular Article

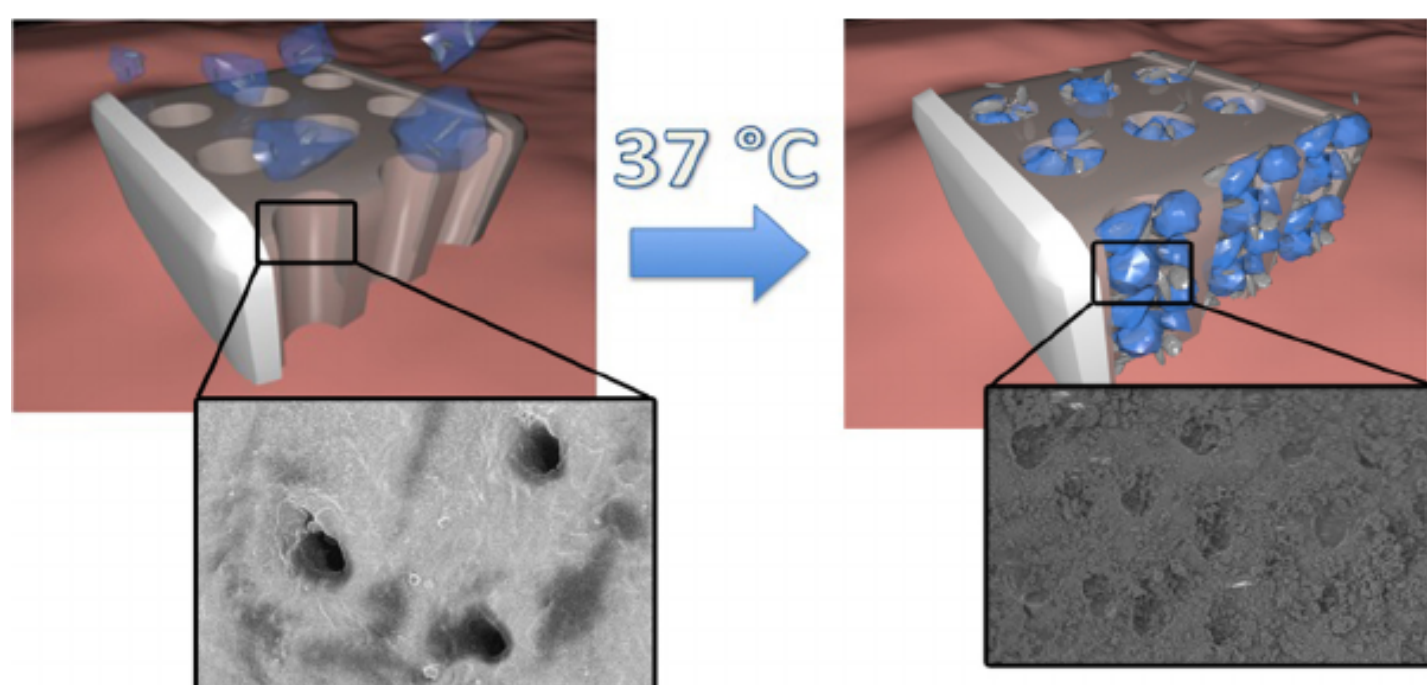
## Poly(N-isopropylacrylamide)-hydroxyapatite nanocomposites as thermoresponsive filling materials on dentinal surface and tubules



Paolo Tempesti, Giovanni Simone Nicotera, Massimo Bonini, Emiliano Fratini\*, Piero Baglioni\*

Department of Chemistry "Ugo Schiff" and CSGI, University of Florence, Via Della Lastruccia 3, 50019 Sesto Fiorentino, Italy

## GRAPHICAL ABSTRACT



## ARTICLE INFO

## Article history:

Received 29 June 2017

Revised 1 September 2017

Accepted 1 September 2017

Available online 21 September 2017

## Keywords:

PNIPAm

Hydroxyapatite

Hydrogel

Microgel

Composite material

Thermoresponsive

Enamel restoration

## ABSTRACT

**Hypothesis:** Dental decay, as a consequence of exposure to acidic foods and drinks, represents one of the most important tooth pathologies. Recently, enamel and dentinal surface remineralization using hydroxyapatite nano- and microparticles has been proposed; however, commercial remineralizing toothpastes are quite expensive, mostly due to the high costs of hydroxyapatite. Hence, we propose a thermoresponsive hybrid nanocomposite material as filler for tooth defects. The use of thermoresponsive composite particles aims at filling exposed dentinal tubules in response to a change of temperature in the oral cavity. In addition, the presence of the organic matrix contributes to the occlusion of the dentinal tubules, therefore reducing the needed amount of hydroxyapatite.

**Experiments:** Poly-N-isopropylacrylamide microgels containing different amounts of hydroxyapatite nanoparticles were prepared via radical polymerization in the presence of N-N-methylenebisacrylamide as cross-linker followed by mechanical grinding. The nano- and microstructure of the hydrogels and their thermal behavior were studied via small-angle X-ray scattering (SAXS), scanning electron microscopy (SEM) and differential scanning calorimetry (DSC). Defected teeth were treated with a dispersion of nanocomposite microparticles to simulate toothpaste action.

**Findings:** The hydrogels maintain their structure and thermal responsiveness when loaded with an amount of hydroxyapatite nanoparticles up to 2.3% w/w. In addition, the lower critical solution temperature is not affected by the presence of the mineral particles. Exposed dentinal tubules on the surface of test tooth samples were successfully occluded after 15 cycles of treatment with a dispersion of nanocomposite microparticles alternated with washing steps.

© 2017 Elsevier Inc. All rights reserved.

\* Corresponding authors.

E-mail addresses: [fratini@csgi.unifi.it](mailto:fratini@csgi.unifi.it) (E. Fratini), [piero.baglioni@unifi.it](mailto:piero.baglioni@unifi.it) (P. Baglioni).

## 1. Introduction

Thermoresponsive polymers are known to exhibit conformational changes because of temperature variations. Block copolymers such as poly(ethylene oxide)-poly(propylene oxide)-poly(ethylene oxide) and poly(N-ethyl oxazoline co-acrylamide), or linear polymers such as poly(N-vinyl caprolactam) and poly-N-isopropylacrylamide (PNIPAm) in water, for instance, undergo a coil-to-globule phase transition from a swollen to a collapsed state when heated above their lower critical solution temperature (LCST) which is typically around or above 32 °C [1–4]. As an example, thermoresponsive polymers, like Pluronic F127 and F68, have been already investigated as delivery systems for various anesthetics targeting the periodontal pocket [2,3]. Together with its biocompatibility [5], the LCST close to the human body temperature represents the main reason for the growing attention on PNIPAm in the biomedical field, especially in view of thermally triggered drug release applications [6]. Recent studies have concluded that no evident collateral effects arise when PNIPAm hydrogels are added to cells [5] even after internalization in lysosomes [7]. Moreover, the cytotoxic response is usually correlated to commercially available PNIPAm where it is likely associated to the presence of impurities in the polymer matrix (monomer, radical initiator) rather than on the polymer itself [5].

PNIPAm is often used as a thermoresponsive matrix in various composite materials, embedding either inorganic or organic micro- and nanoparticles, that are then used in fields such as optics [8,9], chromatographic separation [10], tissue engineering [11] and biomedicine [12]. Among inorganic fillers [13–15], hydroxyapatite (HAP) has attracted most of the interest in the design of synthetic bone replacement materials: in fact, the mineral component of natural bone tissue (which represents 60–70% of its total dry weight) almost entirely consists of HAP [16].

Hydroxyapatite [ $\text{Ca}_{10}(\text{PO}_4)_6(\text{OH})_2$ ] is the main mineral component of teeth as well, constituting the 95% w/w and 75% w/w of enamel and dentin, respectively [17]. HAP is a bio-ceramic that can be resorbed and support the formation of new dental tissue, allowing the tooth to repair its defects, due to its ability of integrating similar chemical structures [18]. It is already been used as a remineralizing agent in commercially available toothpastes, such as UltraDEX<sup>®</sup>, MEGASONEX<sup>®</sup>, or BioRepair<sup>®</sup>. HAP action in those formulations mainly consists in the filling of dentinal tubules whose exposure is due to the partial loss of the enamel layer [19].

Even though the market prices (typically significantly higher than conventional toothpastes) have limited their markets up to now, the advantage in their performances over HAP-free formulations is evident [20]. The high market prices for HAP-containing products are mostly due to production costs of good quality

hydroxyapatite, thus requiring to reduce both HAP costs and amounts needed in the toothpaste to achieve the required effectiveness. In the first case, research has been devoted to obtain hydroxyapatite particles from natural sources with respect to the more expensive synthetic products [21,22], while in the second case there are no reports on the improvement of HAP effectiveness in filling dentinal cavities and further research is required [23].

In this paper, we describe a method for synthesizing a smart nanocomposite material by embedding HAP nanoparticles within PNIPAm hydrogels to improve their adhesion and entrapment within dentinal tubules. While the literature reports few papers where PNIPAm networks are combined with HAP to form composite particles [24–26], to the best of our knowledge there are no scientific reports describing the inclusion of HAP particles within bulk PNIPAm hydrogels. The obtained composite is ground to obtain microparticles whose size fits well that of dentinal tubules. The thermoresponsiveness of the polymeric network introduces a control over the volume occupied and the chemical affinity of the composite particles. The material is designed so that the shrinking of the polymer matrix (triggered by the temperature of the oral cavity) results in the hydrophobization of the nanocomposite and the subsequent sedimentation of the particles on the tooth surface. In addition, the filling of the tubules could be highly enhanced by the reduced size of the particles when in their collapsed state (see Fig. 1). This novel composite material can be readily dispersed in commercial formulations, potentially matching the performances of already existing remineralizing toothpastes, but with reduced costs as a result of the lower amount of HAP needed. Lastly, the thermoresponsiveness of the polymeric network and the potential to release an embedded active molecule could be extended towards different applications, such as pore filling material for on-demand drug releasing membranes [27].

## 2. Experimental

### 2.1. Materials

N-isopropylacrylamide (NIPAm, Sigma-Aldrich, 97%, M.W. 113.16 g/mol), N,N'-methylenebisacrylamide (MBAm, Fluka,  $\geq 98.0\%$ , M.W. 154.17 g/mol), N,N,N',N'-tetramethylethylenediamine (TEMED, Sigma-Aldrich,  $\sim 99\%$ , M.W. 116.2 g/mol) and ammonium persulfate (APS, Sigma-Aldrich,  $\geq 98.0\%$ , M.W. 228.2 g/mol) were used without further purification. Commercial HAP was received as a gift in the form of an aqueous dispersion (NanoXIM CarePaste<sup>®</sup>, Fluidinova S. A., Portugal). The concentration in HAP was 25.5% w/w as obtained by thermogravimetry (see Fig. S1 in the Supplementary Material). Water was purified by a Millipore Organex system ( $R \geq 18 \text{ M}\Omega \text{ cm}$ ).

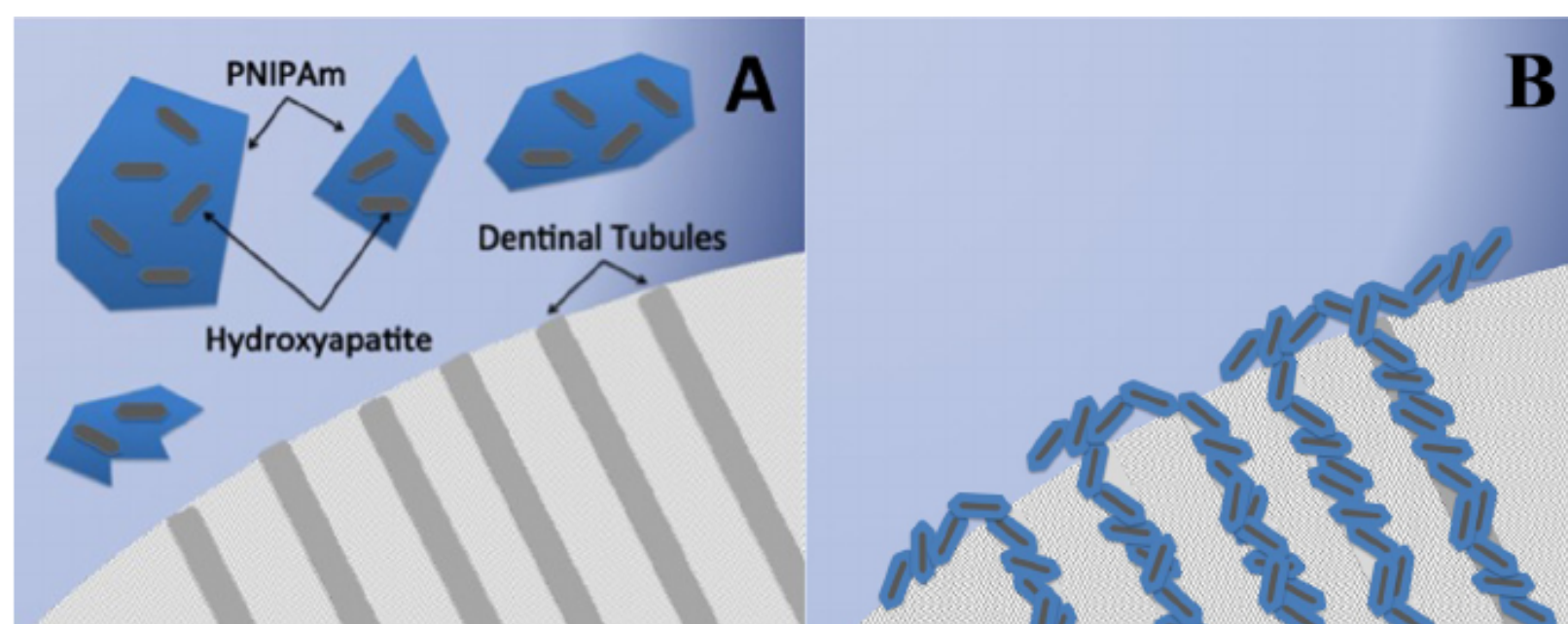


**Fig. 1.** Graphical representation of the proposed work: tooth samples with exposed dentinal tubules are treated with a dispersion of PNIPAm-HAP composite microparticles. At 25 °C the microgel is in its swollen state and hardly enters the tubules (A), while at 37 °C the shrinking leads to the occlusion of the dentinal tubules (B).

## 2.2. Preparation of PNIPAm hydrogels

Aqueous solutions of NIPAm (150 mg/mL), MBAm (5 mg/mL), and APS (4% w/w) were prepared. HAP commercial dispersion was diluted by a factor of 2 and sonicated. All solutions were purged with nitrogen gas to remove solubilized O<sub>2</sub> before polymerization (25 °C for 30 min). Table 1 shows the amounts of reagents used for the preparation of each sample.

## 2.3. Preparation of PNIPAm-HAP microparticles

PNIPAm-HAP composite microgel was prepared by freeze-drying sample H3 and grinding it manually with mortar and pestle. In this way, microparticles with dimensions smaller than dentinal tubules can be obtained. The samples were stored in dry conditions.

## 2.4. Application tests

Adult bovine teeth were chosen as models because of their similar morphology, structure and properties with respect to human teeth [28]. Cylindrical tooth portions (4 mm of diameter and 2 mm of height) were obtained using a drill equipped with a hole saw, and then immobilized in a support of PMMA for dental use (FINODUR®, FINO GmbH). The fragment was positioned with the face of interest resting at the bottom of a cylindrical mold (see Fig. S2). All samples were subjected to a lapping procedure consisting of sequential abrasion with silicon carbide paper (600 and 1200 grit) and alumina abrasive paste (9 μm), each at 18,000 rpm. Between each step, the samples were sonicated in water for 15 min to remove all the debris generated by previous treatments. The specimens were then stored in water. Only the teeth showing exposed dentinal tubules when observed by optical reflection microscopy were selected.

Selected teeth samples have been treated with 20 mL of a 0.5% w/w microparticles dispersion and placed over an orbital shaker at 320 rpm and 37 °C to simulate the temperature in the oral cavity. After 3 h, the dispersion has been recovered and the samples have been washed with water at RT. All samples have been exposed to a total of 15 treatment cycles; *i.e.*, the microparticles have crossed their LCST 15 times.

## 2.5. Field Emission scanning electron microscopy (FE-SEM)

FE-SEM investigation was performed using a ΣIGMA microscope (Carl Zeiss Microscopy GmbH, Germany). A low acceleration potential (1 kV) was used to avoid local charge accumulation effects and secondary electrons were collected by the In-Lens detector. Energy dispersive X-ray analysis (EDX) was performed using a silicon-drift detector X-act (Oxford Instruments), directly coupled with FE-SEM working at an optimal distance of 8.5 mm with an acceleration potential of 5 kV. EDX spectra were processed using the Inca software (Oxford Instruments). The samples were prepared by freezing the hydrogels in their swollen state by direct plunging in liquid nitrogen for 10 min, followed by lyophilization

at about 30 mTorr and –55 °C for 24 h to reach the xerogel state. The solid xerogels were cut with a blade and then finally placed over an aluminum stub covered with conductive tape (internal surface of the xerogel pointing up).

## 2.6. Differential scanning calorimetry (DSC)

DSC curves were obtained with a Q2000 differential scanning calorimeter (TA instruments, Philadelphia, USA). Samples (~15 mg) were placed in cylindrical aluminum hermetic pans. The thermal scan was composed of a first heating ramp from 15 °C to 50 °C, a cooling ramp from 50 °C to 15 °C, and a last ramp identical to the first, all at 3 °C/min. For all experiments a flow of nitrogen of 50 mL/min was maintained. An empty sealed pan was used as reference.

## 2.7. Thermogravimetric analysis (TGA)

TGA measurements were carried out by means of a SDT Q600 (TA instruments, Philadelphia, USA). All scans were performed at a rate of 10 °C/min and a nitrogen flow of 100 mL/min was maintained.

## 2.8. Small angle X-Rays scattering (SAXS)

SAXS experiments were carried out with a Hecus S3- MICRO equipped with a source Genix 50 W microfocus Cu K<sub>α</sub> (λ = 1.54 Å) and one position-sensitive detector (PSD 50 M). Scattering curves were obtained in the *q*-range between 0.009 and 0.54 Å<sup>-1</sup>,  $q = (4\pi/\lambda)\sin\theta$  with *q* scattering vector and 2θ the scattering angle. A thin slice of sample was sealed in a demountable cell with Nalophan® windows and the measurements were performed at controlled temperature from 25 to 40 °C. The measurements were repeated three times for each sample to analyze different areas of the microgels.

The interpretation of the curves was carried out with a simple mathematical model (power laws) associated to the linear regions in the log-log representation:

$$I(q) = Aq^{-p} \quad (1)$$

where *A* is a scale factor and *p* is the slope of the linear fitting. When  $1 \leq p \leq 3$ , *p* represents the mass fractal dimension (*D<sub>m</sub>*) that is 3 for full solid materials [29]. On the other hand, when  $3 \leq p \leq 4$  one can obtain the surface fractal dimension (*D<sub>s</sub>*) from the equation:

$$D_s = 6 - p \quad (2)$$

Typically, *D<sub>s</sub>* is 2 for smooth surfaces, and goes towards 3 as the roughness increases [30].

## 2.9. Dynamic light scattering (DLS)

DLS experiments were performed by means of a Brookhaven 90Plus particle sizer (Brookhaven Instruments Corporation, USA). Auto-correlation functions were analysed using the non-negative least squares (NNLS) algorithm.

**Table 1**

Reagents and amounts used to prepare PNIPAm hydrogels and their LCSTs.

Sample	NIPAm + MBAm solution [mL]	H <sub>2</sub> O [μL]	HAP dispersion [μL]	APS [μL]	TEMED [μL]	HAP in sample [%w/w]	LCST <sup>a</sup> [°C]
H0	1	500	0	100	10	0	33.6
H1	1	450	50	100	10	0.46	33.5
H2	1	400	100	100	10	0.93	33.2
H3	1	250	250	100	10	2.3	32.8
H4	1	0	500	100	10	4.6	32.4

<sup>a</sup> As obtained from DSC measurements.

### 3. Results and discussion

#### 3.1. Morphology of HAP-containing PNIPAm hydrogels

HAP used in this work consisted of nanoparticles ranging from tens to hundreds of nanometers (see Fig. S3 in the Supplementary Material). The effects of the inclusion of HAP nanoparticles on the hydrogel morphology have been studied by means of FE-SEM. Although the morphology of a xerogel is not necessarily representative of that of the hydrogel from which it derives, direct plunging in liquid nitrogen causes the formation of amorphous ice, and the subsequent freeze-drying process has been shown to preserve most of the original morphology [31]. In addition, other methods such as ESEM, critical point drying, and freeze-etching have not proven to be completely reliable in terms of preserving the hydrogel network [32–35]. Micrographs in Fig. 2 show that already at low HAP concentrations (Fig. 2B and C) small modifications in the polymeric network with respect to the bare PNIPAm hydrogel (Fig. 2A) can be noticed. Sample H3 (Fig. 2D) shows a homogeneous dispersion of HAP while the network becomes hardly recognizable. At higher HAP concentrations (Fig. 2E) the regularity of the polymeric matrix is completely lost, and inorganic aggregates of about 100–300 nm are clearly visible.

#### 3.2. Effect of HAP on LCST of PNIPAm hydrogels

It is well known that PNIPAm hydrogels undergo a sol-gel transition upon crossing the LCST [1]. DSC measurements have been performed to verify how the inclusion of HAP nanoparticles in the polymeric matrix affects it. In view of its potential application

as ingredient in toothpastes, the hydrogel LCST should be few degrees lower than the typical oral cavity temperature, *i.e.*, the inclusion of HAP should not significantly change the LCST of PNIPAm. Results in Table 1 show that the LCST is below 37 °C for all samples and slightly decreases while increasing HAP concentration, which is consistent with data reported in the literature [36,37]. It is known that the phase-separation at the LCST depends on the arrangement of water molecules around the hydrophobic residues of the polymer chains [38], so the overall hydrophobization of the hydrogel can be explained considering the removal of water molecules around isopropylamide groups due to hydrogen bonding between the amide proton and the surface phosphate ions of HAP [39]. In addition, the structure-making properties of the ions at the surface of HAP nanoparticles should be pondered. In this view, the Jones-Dole viscosity B-coefficients help in understanding the situation at the surface of HAP particles. In particular, the HAP surface charge plays a key role in the competition between particles and polymer chains for solvation. The Jones-Dole viscosity B-coefficients depend on the ion-solvent interactions, defining the degree of water structuring, and can be positive or negative whether the ionic species possess the tendency to organize (kosmotropic) or disorganize (chaotropic) solvent molecules, respectively [40]. In particular, the presence of ions with a positive B will result in an increase of the hydrophobic interactions between the isopropyl residues on the PNIPAm chains and consequently to a lowering of the LCST. In our case, the ions at the surface of HAP nanoparticles ( $\text{Ca}^{2+}$ ,  $\text{PO}_4^{3-}$  and  $\text{OH}^-$ ) possess B-coefficients of 0.284, 0.590, and 0.122, respectively [41,42], *i.e.*, the presence of HAP in PNIPAm hydrogels is expected to decrease the phase-transition temperature.

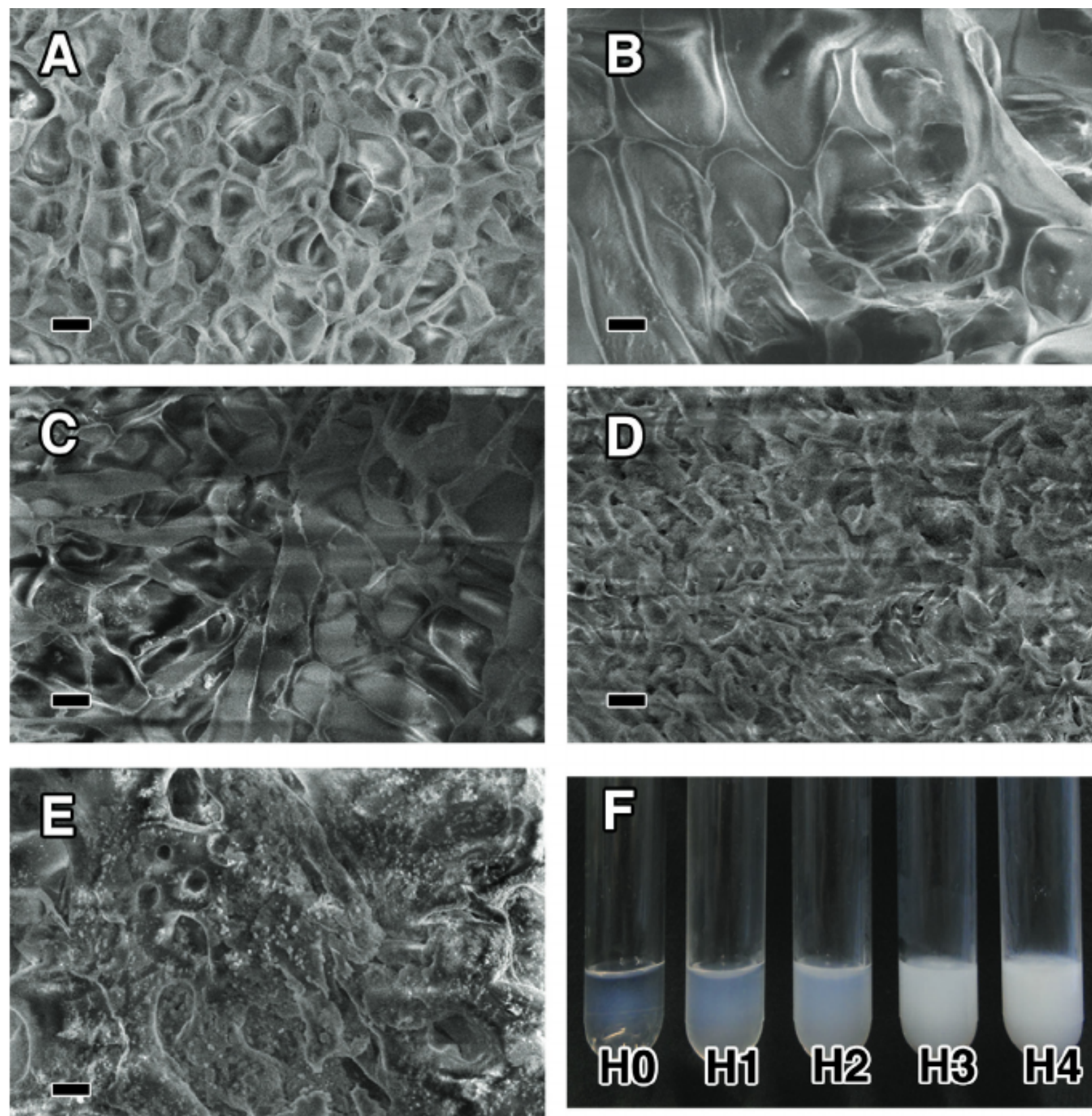
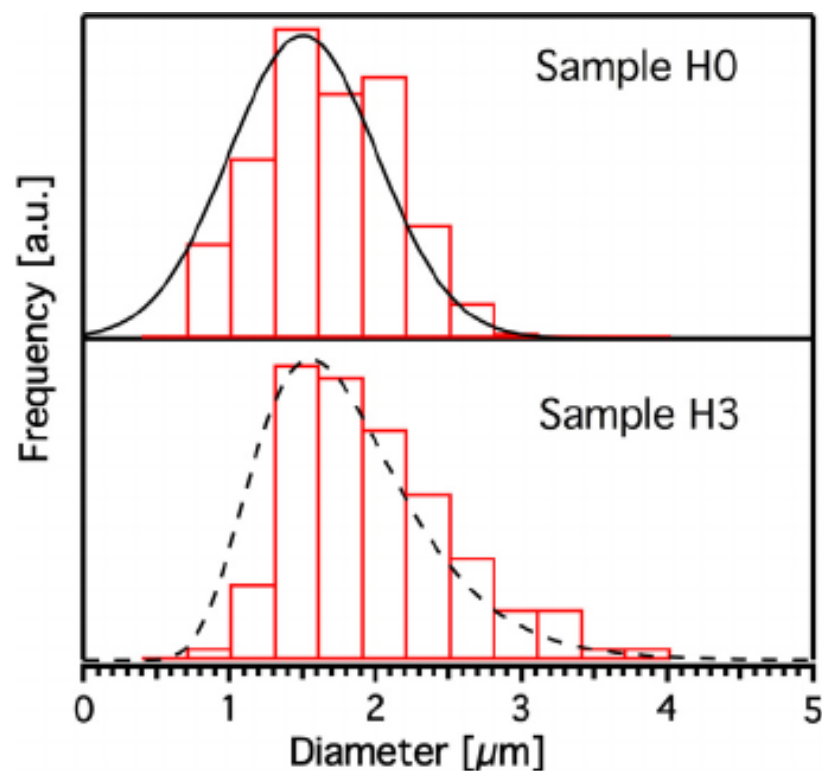


Fig. 2. Representative FE-SEM micrographs of sample H0 (A), H1 (B), H2 (C), H3 (D), and H4 (E) (bar = 2  $\mu\text{m}$ ). (F) Visual aspect of hydrogel samples at 25 °C.

The aim of this work is the design of a homogeneous hydrogel material with the highest amount of embedded HAP particles, still displaying a LCST few degrees below the oral cavity temperature, so that the thermal transition is spontaneously activated when the material is introduced in the mouth. In this framework, the polymer network in sample H4 is nearly lost. Therefore, H3 was chosen as the best candidate and the rest of the paper is focused on a detailed comparison between samples H3 and H0 (chosen as a reference).

### 3.3. Microporosity characterization

The microporosity of H0 and H3 hydrogels was evaluated by measuring the size of at least 150 pores by means of the ImageJ



**Fig. 3.** Pore size distribution of H0 (top) and H3 (bottom) hydrogels. The black solid line and dashed line represent the Gaussian and lognormal size distribution fittings, respectively.

software [43]. Results of the mesh analysis are reported in Fig. 3. From the detailed fit we obtained a mean pore diameter of  $1.51 \pm 0.72 \mu\text{m}$  and  $1.56 \pm 0.44 \mu\text{m}$  for H0 and H3 samples, respectively. HAP inclusion causes a change in the pore size distribution from Gaussian to slightly lognormal while retaining the average pore dimension.

### 3.4. SAXS characterization

SAXS curves were collected to investigate the nanoscale structure of PNIPAm/HAP composites as a function of temperature in the 25–40 °C range, so to highlight the HAP effect on the hydrogel nanostructure around the LCST. The different linear regions in the log-log plot (Fig. 4) were fitted according to a power law approach as described in the experimental section. Sample H0 shows a single linear region and the associated slope increases with temperature. Furthermore, an increase in intensity at  $q > 0.2 \text{ \AA}^{-1}$  is present in all SAXS curves. According to Chalal et al., this feature represents the left side of a correlation peak that for PNIPAm is centered at  $q \sim 0.54 \text{ \AA}^{-1}$ . Its position is almost temperature-independent in the investigated range. The characteristic length associated to this peak can be calculated by means of the Bragg equation,  $d = 2\pi/0.54 = 11.6 \text{ \AA}$ , which is in agreement with the interatomic distance between two isopropyl residues when water molecules are excluded from the polymeric chains (*i.e.* collapsed state) [44]. In addition, the intensity of this peak increases with the temperature, as a consequence of the progressive formation of the hydrophobic domains. In the case of sample H3, all curves exhibit two well-distinct linear regions, while the intensity at  $q \sim 0.55 \text{ \AA}^{-1}$  is again increasing with the temperature. In Table 2,  $p$ ,  $D_m$ , and  $D_s$  values are reported for H0 and H3 samples in the range 25–40 °C.

For both samples  $D_m$  increases with the temperature, confirming that heating leads to a more compact structure as a result of

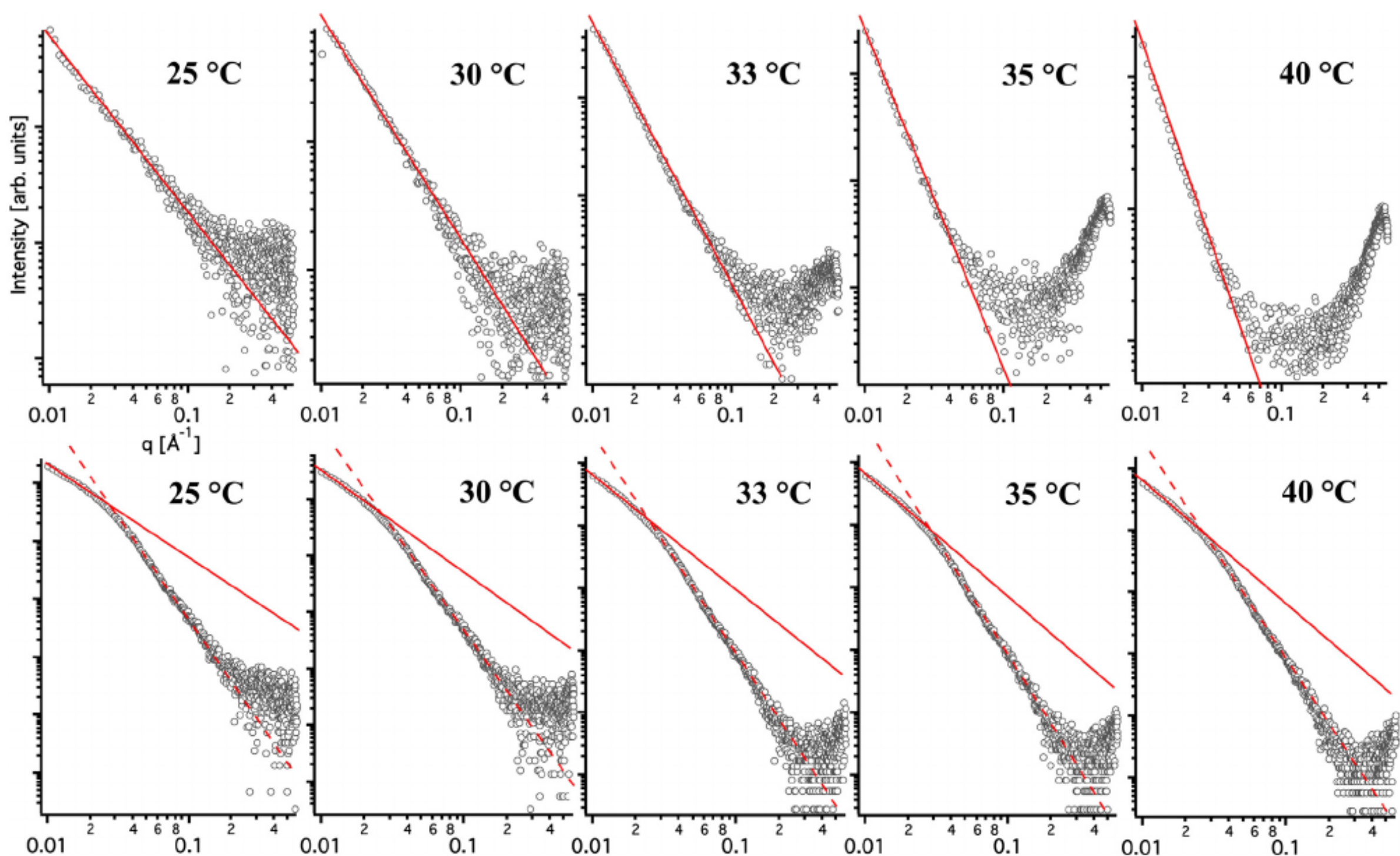


**Fig. 4.** SAXS curves (○) recorded at different temperatures and relative power-law fittings for samples H0 (top) and H3 (bottom).

**Table 2**

Values of the parameters obtained by fitting the SAXS curves with Eq. (1).

Sample H0					Sample H3		
T (°C)	q Range	p	D <sub>m</sub>	D <sub>s</sub>	P	D' <sub>m</sub>	D' <sub>s</sub>
25	Low	1.44 ± 0.05	1.44		1.51 ± 0.05	1.51	2.64
	Med				3.36 ± 0.05		
30	Low	1.76 ± 0.05	1.76		1.67 ± 0.05	1.67	2.52
	Med				3.48 ± 0.06		
33	Low	2.73 ± 0.06	2.73		1.86 ± 0.05	1.86	2.34
	Med				3.66 ± 0.06		
35	Low	2.96 ± 0.07		2.64	1.84 ± 0.05	1.84	2.29
	Med				3.71 ± 0.08		
40	Low	3.06 ± 0.07		2.94	1.92 ± 0.05	1.92	2.28
	Med				3.72 ± 0.07		

the water exclusion from the polymeric matrix. In the case of H0 where only the polymer matrix is present,  $D_m$  increases from 1.44 to 2.73 as the T approaches the LCST from the bottom. At low temperatures, SAXS is probing the local polymer topology in solution (*i.e.* a value of 1.67 is expected in the case of a polymer in a good solvent) [45]. When the temperature is increased above the LCST,  $D_m$  levels at 3 clearly showing that the polymer chains collapse as a result of the transition from a good to a bad solvent. The case of H3 is more complicated to be rationalized since the scattering of HAP superimposes to the one of the polymer matrix. Moreover, if we consider the differences in the scattering length densities of HAP and PNIPAm with regard to water (*i.e.*,  $\text{Ca}_5(\text{PO}_4)_3(\text{OH})$   $2.64 \times 10^{-5} \text{ \AA}^{-2}$ ,  $(\text{C}_6\text{H}_{11}\text{NO})_n$   $1.03 \times 10^{-5} \text{ \AA}^{-2}$  and  $\text{H}_2\text{O}$   $9.46 \times 10^{-6} \text{ \AA}^{-2}$ ) it is clear that the scattering from HAP dominates. For this reason, SAXS curves of H3 are mainly associated with the inhomogeneities in the 1–50 nm range proper of the HAP dispersion in the polymer matrix. Objects larger than 50 nm cannot be investigated due to the experimental resolution associated with the SAXS set-up. For this reason, the fitting of the complete curve with a detailed model was not carried out. As a simpler approach, we can describe the global curve with two linear regions one in the low  $q$  ( $0.01\text{--}0.03 \text{ \AA}^{-1}$ ) and one in the medium  $q$  regime ( $0.03\text{--}0.3 \text{ \AA}^{-1}$ ) and extract two “apparent” fractal dimensions  $D'_m$  and  $D'_s$ , respectively. We refer to them as “apparent” for two reasons: the scattering curve is not complete at low  $q$  and moreover, the scattering signal comes from both HAP and PNIPAm. The

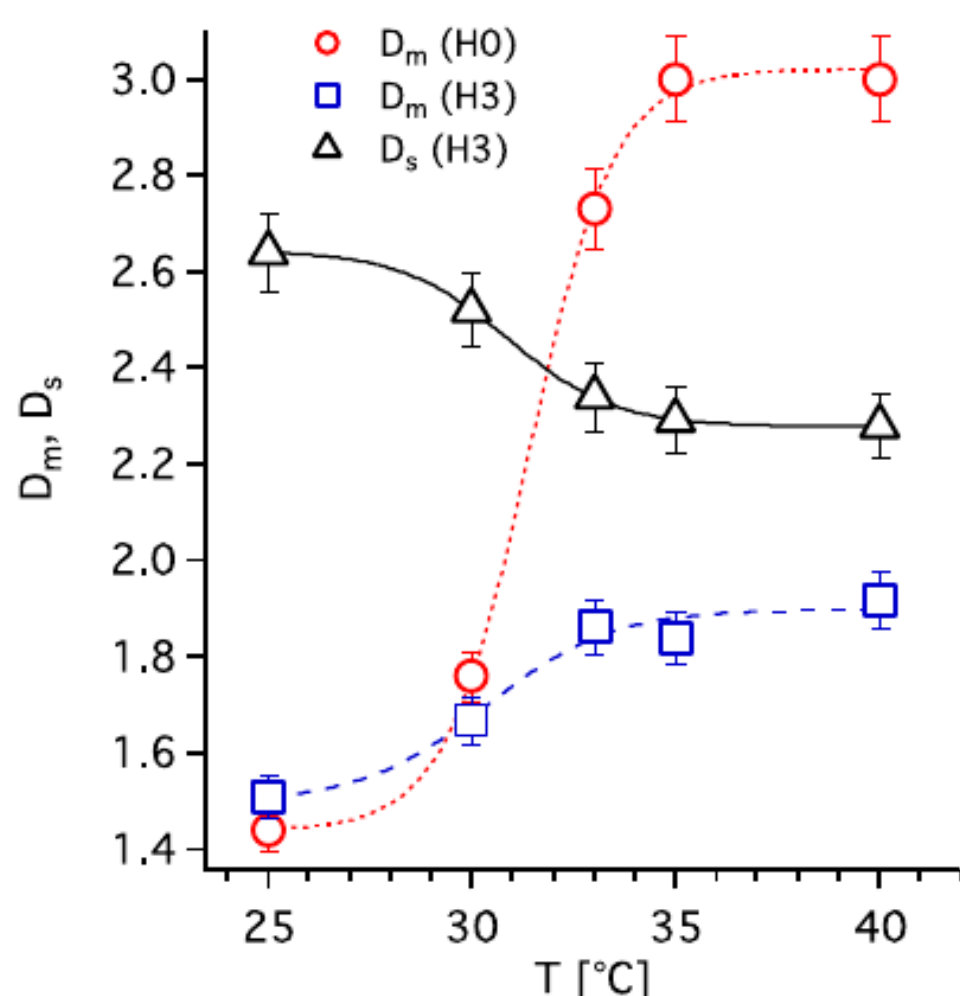
differences in fractal dimensions evidenced when the temperature is increased are strictly linked to the variation in the topology of PNIPAm surrounding HAP particles. In particular,  $D'_m$ , describing the low  $q$  regime, changes from 1.51 to 1.92 as a result of the collapse of PNIPAm on top of the inorganic material. In the case of  $D'_s$ , its value changes from 2.64 to 2.28 showing that the increase in T reduces the roughness of the surface as a result of the polymer contraction on the HAP nanoparticles. Notably, D variations in all the cases (H0 and H3) are always sigmoidal and in agreement with a temperature induced transition at about 32 °C (see Fig. 5).

### 3.5. Microparticles Preparation

The aforementioned results confirmed that the PNIPAm/HAP composites with up to 2.3% w/w of HAP maintain the structural and thermoresponsive properties of the pure hydrogel. Aiming at employing the hydrogel in the thermally enhanced filling of exposed dentinal tubules, the xerogel obtained by freeze-drying sample H3 has been frozen again and then grinded with a mortar and pestle and eventually dispersed in water to obtain a 0.1% w/w dispersion. Fig. 6A shows FE-SEM images of the obtained powder. Due to the grinding process, the particles exhibit various shapes and dimensions, ranging from hundreds of nanometers to tens of microns. At higher magnifications HAP nanoparticles are visible and their presence is also confirmed by EDX analysis since the calculated Ca/P ratio, as reported in Table 3, is similar to that of HAP (see also Fig. S4 in the Supplementary Material).

### 3.6. Thermal responsivity of microparticles

The DSC curve in Fig. 6B shows that, despite the dimensions of the particles, a LCST transition is still present and it is not affected by thermal cycles, as confirmed by the superposition of the heating portion of the curves. To investigate the change of the dimensions of the composite microparticles associated to the LCST, particles with dimensions in the sub-micrometer range were selected by sedimentation and then investigated by means of dynamic light scattering (DLS). This size selection was performed because the range of sizes accurately accessible by DLS is limited to a maximum of about 1  $\mu\text{m}$ . Fig. 6C shows the size distributions obtained from the analysis of the auto-correlation functions (see Fig. S5 in the Supplementary Material) at 30 °C ( $T < \text{LCST}$ ) and 35 °C ( $T > \text{LCST}$ ) according to the NNLS algorithm. Below the LCST a single distribution centered slightly below 1  $\mu\text{m}$  in diameter is obtained, demonstrating that the size selection procedure was successful. Above the LCST a population centered at about 240 nm is present, together with a distribution centered at about 850 nm. In both samples, residues of sedimentation with diameters higher than 4  $\mu\text{m}$  are present (not shown in Fig. 6C). From these results it

**Fig. 5.** Variation of characteristic fractal dimensions for samples H0 and H3.

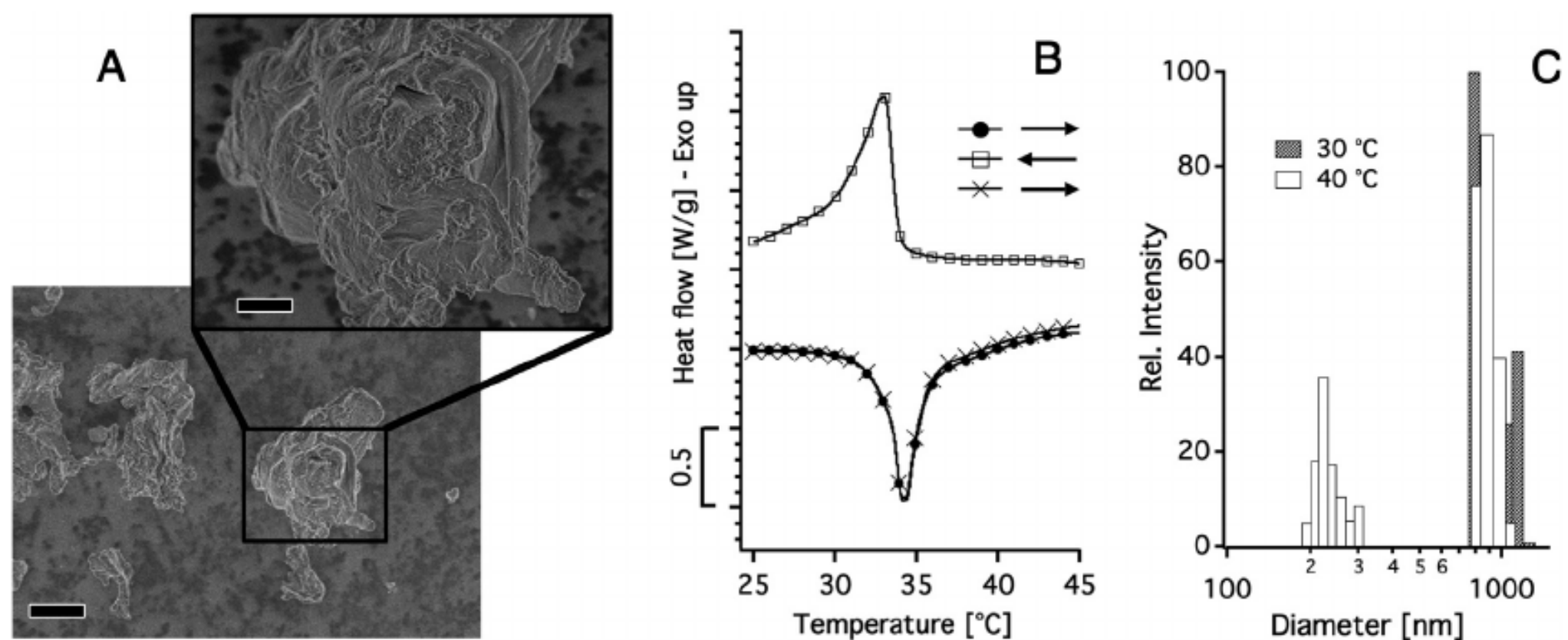


**Fig. 6.** (A) FE-SEM images of freeze-dried H3 sample after grinding (bar = 5  $\mu\text{m}$ ; inset bar = 1  $\mu\text{m}$ ). (B) DCS thermogram of H3 microparticles. (C) Particle size distribution of H3 microparticles as obtained by DLS. Populations higher than 1500 nm are not displayed.

**Table 3**

Comparison between the theoretical and experimental HAP Ca/P ratio.

HAP Ca/P ratio (theoretical)	1.67
HAP Ca/P ratio (from EDX)	$1.79 \pm 0.20$

is evident that while raising the temperature above the LCST the dimensions of the particles diminish by a factor of about 4 and the increase of the hydrophobic interactions between the collapsed particles leads to the formation of aggregates, in agreement with previous studies [46].

### 3.7. Application tests

Application tests of the dispersion of PNIPAm/HAP microparticles were performed on adult bovine teeth specimens, since they are similar in morphology and possess properties comparable to those of humans [28]. Taking into account that the smallest size of dentinal tubules typically approaches 1–2  $\mu\text{m}$  [47], and that the temperature range in a human mouth typically ranges between 33.2 °C and 38.2 °C [48], when the composite microgels experience a temperature higher than LCST, they are small enough (about

200 nm) to easily enter and fill the tubules. On the other hand, the particles in their cold state (below the LCST) can grow so to remain entrapped within the tubules in case a decrease in temperature is experienced inside the mouth. It is important to stress that, in the framework of their application in the oral cavity, the particles would typically be in their collapsed state. When eating or drinking cold beverages or foods, the variations of temperature in the oral cavity are more pronounced [49], so the particles will be subjected to several swell-collapse transitions at the end of the eating/drinking process. On the other hand, no change will take place in their structure when eating or drinking something warm. The deposition procedure consisted of alternated treatment/washing cycles, as reported in Fig. 7A. FE-SEM images were collected before and after the deposition. Fig. 7B and C show the non-treated tooth sample with exposed dentinal tubules, while in Fig. 7D and E the effects of the deposition treatment on the samples are presented.

The surface of treated samples appears covered in particles and the tubules are partially filled. While observing the structure of the deposit, it appears that the composite particles, in addition to their binding with the tooth matrix, also form aggregates. This may be due to the fact that the affinity between the tooth and the composite increases when increasing the temperature, because of the

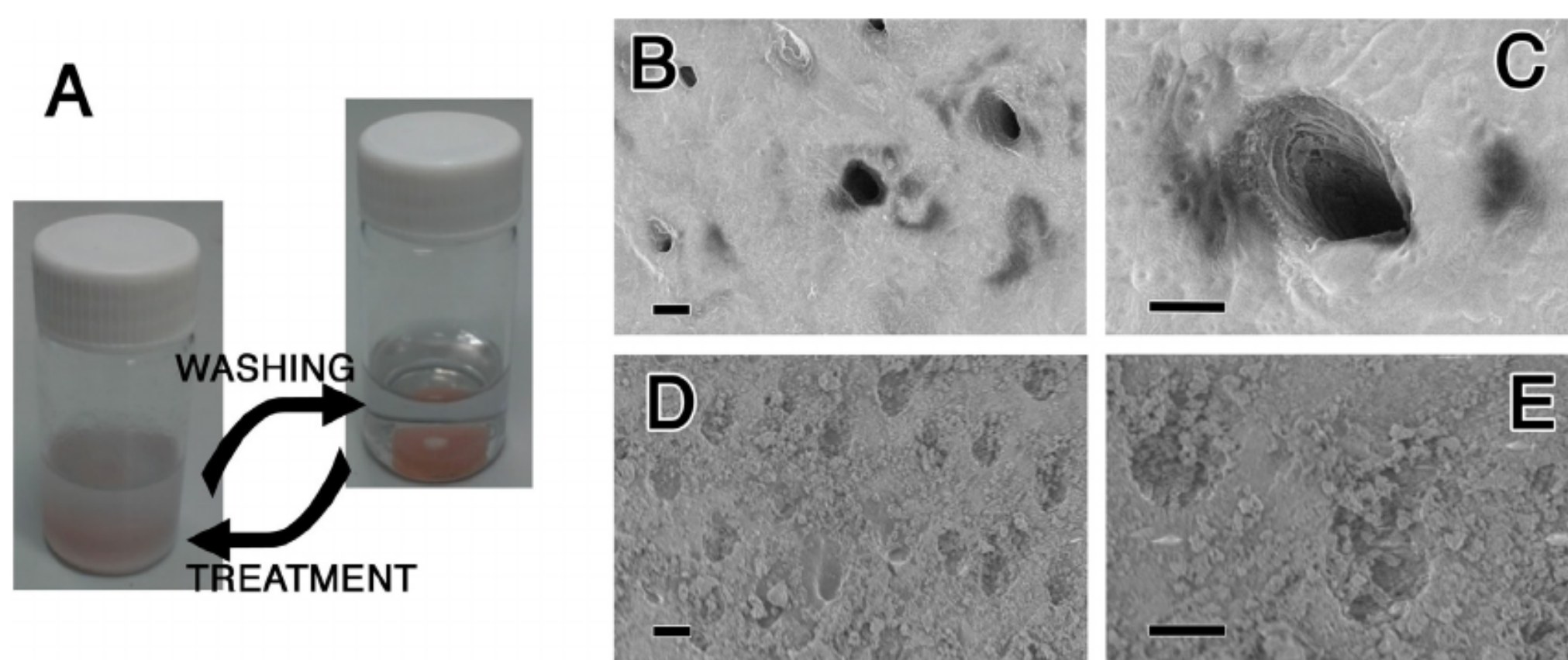


**Fig. 7.** (A) Tooth sample aspect during the treatment with the composite microparticles dispersion, and the washing step. FE-SEM micrographs of bovine tooth specimens before (B, C) and after (D, E) the treatment with H3 microgel (bar = 2  $\mu\text{m}$ ). Higher magnifications evidence the presence of particles inside the dentinal tubules (D, bar = 1  $\mu\text{m}$ ).

appearance of a great number of hydrophobic interactions causing a decrease in the stability of the dispersion and thus accelerating the deposition process. Furthermore, in spite of the swelling/shrinking cycles experienced by the material, the deposit shows no sign of cracking, highlighting the mechanical resistance of the composite towards thermal stresses.

#### 4. Conclusions

We described the synthesis, characterization and application of a hybrid responsive material consisting of HAP nanoparticles embedded in a PNIPAm microgel suitable for the occlusion of dentinal tubules. PNIPAm represents a perfect case study for this application because of its LCST close to the average temperature of the oral cavity. Different PNIPAm/HAP composites are studied varying the amount of the inorganic content. The structural and responsive properties of the pure PNIPAm hydrogel were maintained when the HAP content was up to 2.3% w/w with respect to the polymer. The selected sample was freeze-dried, ground with mortar and pestle so to obtain a powder containing composite microparticles, which was eventually dispersed in water for deposition tests on adult bovine teeth. The LCST of PNIPAm allows the size reduction of the composite in mouth so that it is possible, even starting with micro-size domains, to deliver sub-micron objects able to enter and fill exposed tubules. Moreover, during the transition from the cold state to the warm state the composite becomes more hydrophobic and the interaction with the surface is favored. This temperature dependent responsiveness can also be used to deliver actives directly in the mouth. After the treatment, exposed dentinal tubules were not present any longer, being efficiently filled with the PNIPAm/HAP particles. Differently from thermoresponsive drug delivery systems based on physical gels [2,3], using a chemical thermoresponsive hydrogel as scaffold for HAP offers the advantages of controlling the remineralizing process and the potential release of an active through the application of an external *stimulus*. Furthermore, these mechanically stable microparticles could be easily introduced in toothpastes, lowering the amount of the needed inorganic component and potentially reducing the final costs of the commercial product while adding new functionalities to the final formulation. As a last remark, it is important to stress that the concept illustrated in this work could be easily achieved using any similar system with LCST between 30 and 35 °C. Examples could be chemical gels based on members of the Pluronic® class, poly(N-ethyl oxazoline co-acrylamide), poly(N-vinyl caprolactam), and elastin-like polypeptides.

#### Acknowledgment

Financial support from CSGI is acknowledged.

#### Author contributions

The manuscript was written through contributions of all authors. All authors have given approval to the final version of the manuscript.

#### Appendix A. Supplementary material

TGA of NanoXIM Care Paste HAP (Fig. S1). Image of specimen for deposition tests (Fig. S2). FE-SEM image of HAP (Fig. S3). EDX analysis on composite microparticles (Fig. S4). DLS correlation functions (Fig. S5). Supplementary data associated with this article can be found, in the online version, at <http://dx.doi.org/10.1016/j.jcis.2017.09.001>.

#### References

- [1] M.J. Snowden, B.Z. Chowdhry, B. Vincent, G.E. Morris, Colloidal copolymer microgels of N-isopropylacrylamide and acrylic acid: pH, ionic strength and temperature effects, *J. Chem. Soc. Faraday Trans. 92* (1996) 5013–5016, <http://dx.doi.org/10.1039/FT9969205013>.
- [2] N.A. Cortez-Lemus, A. Licea-Claverie, Poly(N-vinylcaprolactam), a comprehensive review on a thermoresponsive polymer becoming popular, *Prog. Polym. Sci.* 53 (2016) 1–51, <http://dx.doi.org/10.1016/j.progpolymsci.2015.08.001>.
- [3] M. Scherlund, M. Malmsten, P. Holmqvist, A. Brodin, Thermosetting microemulsions and mixed micellar solutions as drug delivery systems for periodontal anesthesia, *Int. J. Pharm.* 194 (2000) 103–116, [http://dx.doi.org/10.1016/S0378-5173\(99\)00366-X](http://dx.doi.org/10.1016/S0378-5173(99)00366-X).
- [4] M. Scherlund, A. Brodin, M. Malmsten, Micellization and gelation in block copolymers systems containing local anesthetics, *Int. J. Pharm.* 211 (2000) 37–49, [http://dx.doi.org/10.1016/S0378-5173\(00\)00589-5](http://dx.doi.org/10.1016/S0378-5173(00)00589-5).
- [5] M.A. Cooperstein, H.E. Canavan, Assessment of cytotoxicity of (N-isopropyl acrylamide) and Poly(N-isopropyl acrylamide)-coated surfaces, *Biointerphases* 8 (2013), <http://dx.doi.org/10.1186/1559-4106-8-19>.
- [6] D. Schmaljohann, Thermo- and pH-responsive polymers in drug delivery, *Adv. Drug Deliv. Rev.* 58 (2006) 1655–1670, <http://dx.doi.org/10.1016/j.addr.2006.09.020>.
- [7] P.C. Naha, K. Bhattacharya, T. Tenuta, K.A. Dawson, I. Lynch, A. Gracia, F.M. Lyng, H.J. Byrne, Intracellular localisation, geno- and cytotoxic response of poly N-isopropylacrylamide (PNIPAM) nanoparticles to human keratinocyte (HaCaT) and colon cells (SW 480), *Toxicol. Lett.* 198 (2010) 134–143, <http://dx.doi.org/10.1016/j.toxlet.2010.06.011>.
- [8] M. Zhang, N.I. Rabiah, T.H. Ngo, T.P. Otanicar, P.E. Phelan, R. Swaminathan, L.L. Dai, Thermo-responsiveness and tunable optical properties of asymmetric polystyrene/PNIPAM-gold composite particles, *J. Colloid Interface Sci.* 425 (2014) 12–19, <http://dx.doi.org/10.1016/j.jcis.2014.03.017>.
- [9] F.Y. Pong, M. Lee, J.R. Bell, N.T. Flynn, Thermoresponsive behavior of poly(N-isopropylacrylamide) hydrogels containing gold nanostructures, *Langmuir* 22 (2006) 3851–3857, <http://dx.doi.org/10.1021/la0534165>.
- [10] N. Shamim, L. Hong, K. Hidajat, M.S. Uddin, Thermosensitive polymer coated nanomagnetic particles for separation of bio-molecules, *Sep. Purif. Technol.* 53 (2007) 164–170, <http://dx.doi.org/10.1016/j.seppur.2006.06.021>.
- [11] R.M.P. da Silva, J.F. Mano, R.L. Reis, Smart thermoresponsive coatings and surfaces for tissue engineering: switching cell-material boundaries, *Trends Biotechnol.* 25 (2007) 577–583, <http://dx.doi.org/10.1016/j.tibtech.2007.08.014>.
- [12] S. Chaterji, I.K. Kwon, K. Park, Smart polymeric gels: redefining the limits of biomedical devices, *Prog. Polym. Sci.* 32 (2007) 1083–1122, <http://dx.doi.org/10.1016/j.progpolymsci.2007.05.018>.
- [13] G. Huyang, A.E. Debertin, J. Sun, Design and development of self-healing dental composites, *Mater. Des.* 94 (2016) 295–302, <http://dx.doi.org/10.1016/j.matdes.2016.01.046>.
- [14] M.M. Taheri, M.R. Abdul Kadir, T. Shokuhfar, A. Hamlekhan, M.R. Shirdar, F. Naghizadeh, Fluoridated hydroxyapatite nanorods as novel fillers for improving mechanical properties of dental composite: synthesis and application, *Mater. Des.* 82 (2015) 119–125, <http://dx.doi.org/10.1016/j.matdes.2015.05.062>.
- [15] B. Yu, H.-N. Lim, Y.-K. Lee, Influence of nano- and micro-filler proportions on the optical property stability of experimental dental resin composites, *Mater. Des.* 31 (2010) 4719–4724, <http://dx.doi.org/10.1016/j.matdes.2010.05.019>.
- [16] R.P. Heaney, R.R. Recker, P. Watson, J.M. Lappe, Phosphate and carbonate salts of calcium support robust bone building in osteoporosis, *Am. J. Clin. Nutr.* 92 (2010) 101–105, <http://dx.doi.org/10.3945/ajcn.2009.29085>.
- [17] N. Roveri, E. Battistella, C.L. Bianchi, I. Foltran, E. Foresti, M. Iafisco, M. Lelli, A. Naldoni, B. Palazzo, L. Rimondini, Surface enamel remineralization: biomimetic apatite nanocrystals and fluoride ions different effects, *J. Nanomater.* 2009 (2009) e746383, <http://dx.doi.org/10.1155/2009/746383>.
- [18] G.P. Jayaswal, S.P. Dange, A.N. Khalikar, Bioceramic in dental implants: a review, *J. Indian Prosthodont. Soc.* 10 (2010) 8–12, <http://dx.doi.org/10.1007/s13191-010-0002-4>.
- [19] K. Ishikawa, T. Suge, M. Yoshiyama, A. Kawasaki, K. Asaoka, S. Ebisu, Occlusion of dentinal tubules with calcium phosphate using acidic calcium phosphate solution followed by neutralization, *J. Dent. Res.* 73 (1994) 1197–1204, <http://dx.doi.org/10.1177/00220345940730061101>.
- [20] M. Lelli, A. Putignano, M. Marchetti, I. Foltran, F. Mangani, M. Procaccini, N. Roveri, G. Orsini, Remineralization and repair of enamel surface by biomimetic Zn-carbonate hydroxyapatite containing toothpaste: a comparative in vivo study, *Front. Physiol.* 5 (2014), <http://dx.doi.org/10.3389/fphys.2014.00333>.
- [21] M. Adak, K.M. Purohit, Synthesis of nano-crystalline hydroxyapatite from dead snail shells for biological implantation, *Trends Biomater. Artif. Organs* 25 (2011) 101–106.
- [22] J. Zhang, D. Jiang, J. Zhang, Q. Lin, Z. Huang, Synthesis of dental enamel-like hydroxyapatite through solution mediated solid-state conversion, *Langmuir* 26 (2010) 2989–2994, <http://dx.doi.org/10.1021/la9043649>.
- [23] M. Hannig, C. Hannig, Nanomaterials in preventive dentistry, *Nat. Nanotechnol.* 5 (2010) 565–569, <http://dx.doi.org/10.1038/nnano.2010.83>.
- [24] J.C. Wei, Y.F. Dai, Y.W. Chen, Synthesis and characterization of a new type of smart hydroxyapatite-PNIPAM hybrid nanoparticles, *Adv. Mater. Res.* 396–398 (2011) 35–39, <http://dx.doi.org/10.4028/www.scientific.net/AMR.396-398.35>.

- [25] J. Wei, P. He, A. Liu, X. Chen, X. Wang, X. Jing, Surface modification of hydroxyapatite nanoparticles with thermal-responsive PNIPAM by ATRP, *Macromol. Biosci.* 9 (2009) 1237–1246, <http://dx.doi.org/10.1002/mabi.200900256>.
- [26] Y. Yu, H. Zhang, H. Sun, D. Xing, F. Yao, Nano-hydroxyapatite formation via coprecipitation with chitosan-g-poly(N-isopropylacrylamide) in coil and globule states for tissue engineering application, *Front. Chem. Sci. Eng.* 7 (2013) 388–400, <http://dx.doi.org/10.1007/s11705-013-1355-0>.
- [27] T. Hoare, J. Santamaria, G.F. Goya, S. Irusta, D. Lin, S. Lau, R. Padera, R. Langer, D. S. Kohane, A magnetically triggered composite membrane for on-demand drug delivery, *Nano Lett.* 9 (2009) 3651–3657, <http://dx.doi.org/10.1021/nl9018935>.
- [28] G.H. Yassen, J.A. Platt, A.T. Hara, Bovine teeth as substitute for human teeth in dental research: a review of literature, *J. Oral Sci.* 53 (2011) 273–282.
- [29] B. Hammouda, Probing Nanoscale Structures – The SANS Toolbox. <[http://www.ncnr.nist.gov/staff/hammouda/the\\_SANS\\_toolbox.pdf](http://www.ncnr.nist.gov/staff/hammouda/the_SANS_toolbox.pdf)>, (n.d.) (accessed August 4, 2015).
- [30] D.W. Schaefer, Fractal models and the structure of materials, *MRS Bull.* 13 (1988) 22–27, <http://dx.doi.org/10.1557/S088376940006632X>.
- [31] S. Paterson, Y. Casadio, D. Brown, J. Shaw, T.V. Chirila, M. Baker, Laser scanning confocal microscopy versus scanning electron microscopy for characterization of polymer morphology: sample preparation drastically distorts morphologies of poly(2-hydroxyethyl methacrylate)-based hydrogels, *J. Appl. Polym. Sci.* 127 (2013) 4296–4304, <http://dx.doi.org/10.1002/app.38034>.
- [32] L.-M. Joubert, Visualization of hydrogels with variable-pressure SEM, *Microsc. Microanal.* 15 (2009) 1308–1309, <http://dx.doi.org/10.1017/S1431927609096263>.
- [33] D. Bray, Critical point drying of biological specimens for scanning electron microscopy, in: J. Williams, A. Clifford (Eds.), *Supercrit. Fluid Methods Protoc.*, Humana Press, 2000, pp. 235–243. <<http://dx.doi.org/10.1385/1-59259-030-6%3A235>> (accessed March 6, 2017).
- [34] B.G. Nordestgaard, J. Rostgaard, Critical-point drying versus freeze drying for scanning electron microscopy: a quantitative and qualitative study on isolated hepatocytes, *J. Microsc.* 137 (1985) 189–207.
- [35] L. Qian, H. Zhang, Controlled freezing and freeze drying: a versatile route for porous and micro-/nano-structured materials, *J. Chem. Technol. Biotechnol.* 86 (2011) 172–184, <http://dx.doi.org/10.1002/jctb.2495>.
- [36] M.-T. Nistor, D. Pamfil, C. Schick, C. Vasile, Study of the heat-induced denaturation and water state of hybrid hydrogels based on collagen and poly(N-isopropyl acrylamide) in hydrated conditions, *Thermochim. Acta* 589 (2014) 114–122, <http://dx.doi.org/10.1016/j.tca.2014.05.020>.
- [37] L. Ioan, M. Teodorescu, P.O. St nescu, C. Drăghici, A. Zaharia, A. Sârbu, S. Stoleriu, The effect of hydrophilic bentonite nanoclay on the thermogelation properties of poly(N-isopropylacrylamide)-poly(ethylene glycol)-poly(N-isopropylacrylamide) triblock copolymer aqueous solutions, *J. Macromol. Sci. Part B* 54 (2015) 316–328, <http://dx.doi.org/10.1080/00222348.2015.1010419>.
- [38] R. Freitag, F. Garret-Flaudy, Salt effects on the thermoprecipitation of poly-(N-isopropylacrylamide) oligomers from aqueous solution, *Langmuir* 18 (2002) 3434–3440, <http://dx.doi.org/10.1021/la0106440>.
- [39] H. Zhang, F. Li, B. Dever, C. Wang, X.-F. Li, X.C. Le, Assembling DNA through affinity binding to achieve ultrasensitive protein detection, *Angew. Chem. Int. Ed.* 52 (2013) 10698–10705, <http://dx.doi.org/10.1002/anie.201210022>.
- [40] G. Jones, M. Dole, *J. Am. Chem. Soc.* (1929) 2950.
- [41] A.S. Parmar, M. Muschol, Hydration and hydrodynamic interactions of lysozyme: effects of chaotropic versus kosmotropic ions, *Biophys. J.* 97 (2009) 590–598, <http://dx.doi.org/10.1016/j.bpj.2009.04.045>.
- [42] H.D.B. Jenkins, Y. Marcus, Viscosity B-coefficients of ions in solution, *Chem. Rev.* 95 (1995) 2695–2724, <http://dx.doi.org/10.1021/cr00040a004>.
- [43] C.A. Schneider, W.S. Rasband, K.W. Eliceiri, NIH image to imageJ: 25 years of image analysis, *Nat. Methods* 9 (2012) 671–675, <http://dx.doi.org/10.1038/nmeth.2089>.
- [44] M. Chalal, F. Ehrburger-Dolle, I. Morfin, F. Bley, M.-R. Aguilar de Armas, M.-L. López, J. San Donaire, N. Roman, E. Bölgen, O. Piskin, R. Casalegno Ziane, SAXS investigation of the effect of temperature on the multiscale structure of a macroporous poly(N-isopropylacrylamide) gel, *Macromolecules* 43 (2010) 2009–2017, <http://dx.doi.org/10.1021/ma902655h>.
- [45] E. Carretti, L. Dei, A. Macherelli, R.G. Weiss, Rheoreversible polymeric organogels: the art of science for art conservation, *Langmuir* 20 (2004) 8414–8418, <http://dx.doi.org/10.1021/la0495175>.
- [46] C. Wu, X. Wang, Globule-to-coil transition of a single homopolymer chain in solution, *Phys. Rev. Lett.* 80 (1998) 4092–4094, <http://dx.doi.org/10.1103/PhysRevLett.80.4092>.
- [47] R. Schilke, J.A. Lisson, O. Bauß, W. Geurtsen, Comparison of the number and diameter of dentinal tubules in human and bovine dentine by scanning electron microscopic investigation, *Arch. Oral Biol.* 45 (2000) 355–361, [http://dx.doi.org/10.1016/S0003-9969\(00\)00006-6](http://dx.doi.org/10.1016/S0003-9969(00)00006-6).
- [48] M. Sund-Levander, C. Forsberg, L.K. Wahren, Normal oral, rectal, tympanic and axillary body temperature in adult men and women: a systematic literature review, *Scand. J. Caring Sci.* 16 (2002) 122–128, <http://dx.doi.org/10.1046/j.1471-6712.2002.00069.x>.
- [49] B.H. Newman, C.A. Martin, The effect of hot beverages, cold beverages, and chewing gum on oral temperature, *Transfusion (Paris)*. 41 (2001) 1241–1243, <http://dx.doi.org/10.1046/j.1537-2995.2001.41101241.x>.